Near-Infrared SERS Nanoprobes with Plasmonic Au/Ag Hollow-Shell Assemblies for In Vivo Multiplex Detection

Homan Kang, Sinyoung Jeong, Younggeun Park, Joonhyuk Yim, Bong-Hyun Jun, San Kyeong, Jin-Kyoung Yang, Gunsung Kim, SoonGweon Hong, Luke P. Lee, Jong-Ho Kim, Ho-Young Lee,* Dae Hong Jeong,* and Yoon-Sik Lee**

For the effective application of surface-enhanced Raman scattering (SERS) nanoprobes for in vivo targeting, the tissue transparency of the probe signals should be as high as it can be in order to increase detection sensitivity and signal reproducibility. Here, near-infrared (NIR)-sensitive SERS nanoprobes (NIR SERS dots) are demonstrated for in vivo multiplex detection. The NIR SERS dots consist of plasmonic Au/Ag hollow-shell (HS) assemblies on the surface of silica nanospheres and simple aromatic Raman labels. The diameter of the HS interior is adjusted from 3 to 11 nm by varying the amount of Au^{3+} added, which results in a red-shift of the plasmonic extinction of the Au/Ag nanoparticles toward the NIR (700–900 nm). The red-shifted plasmonic extinction of NIR SERS dots causes enhanced SERS signals in the NIR optical window where endogenous tissue absorption coefficients are more than two orders of magnitude lower than those for ultraviolet and visible light. The signals from NIR SERS dots are detectable from 8-mm deep in animal tissues. Three kinds of NIR SERS dots, which are injected into live animal tissues, produce strong SERS signals from deep tissues without spectral overlap, demonstrating their potential for in vivo multiplex detection of specific target molecules.

1. Introduction

Molecular imaging holds potential as a tool for discovering the basic functions of biological molecules and the mechanisms of various diseases.[1] Among many molecular imaging techniques, optical imaging has gained much attention in biology, medicine, and nanobiotechnology due to advantages including the lack of a radioactivity hazard, higher sensitivity, improved spatial resolution, and better high-throughput capability.[2] However, in vivo optical imaging applications have been hampered by low penetrating capability of optical signals as in the case of organic fluorescent dyes against animal's deep tissues of emanating autofluorescence, resulting in lowering sensitivity and signal reproducibility.[1,2] Optical probes producing signals in the near-infrared (NIR) window region (700–900 nm), where endogenous tissue absorption coefficients are more than two orders of magnitude lower than those for ultra-violet and visible light, have been considered suitable candidates for in vivo applications.[3] Several types of optical probes emitting NIR photoluminescence such as NIR fluorescence dyes,[4] carbon nanotubes,[5] and quantum dots (QDs)[6] have been used to detect and image biomolecules in vivo. However, they still have some limitations such as photobleaching, cytotoxicity, and the limited number of distinct fluorescence signals in the NIR window.[7,8]

H. Kang, Prof. D. H. Jeong, Prof. Y.-S. Lee
Nano Systems Institute and Interdisciplinary Program in Nano-Science and Technology
Seoul National University
Seoul, 151-742, Republic of Korea
E-mail: jeongdh@snu.ac.kr; yslee@snu.ac.kr
S. Jeong, G. Kim, Prof. D. H. Jeong
Department of Chemistry Education
Seoul National University
Seoul, 151-742, Republic of Korea
Dr. Y. Park, Dr. S. G. Hong, Prof. L. P. Lee
Department of Bioengineering
University of California Berkeley
Berkeley, CA 94720, USA
J. Yim, S. Kyoeng, J.-K. Yang, Prof. Y.-S. Lee
School of Chemical and Biological Engineering
Seoul National University
Seoul 151-742, Republic of Korea
Prof. B.-H. Jun
Department of Bioscience and Biotechnology
Konkuk University
Seoul 143-701, Republic of Korea
Prof. J.-H. Kim
Department of Chemical Engineering
Hanyang University, Ansan
426-791, Republic of Korea
E-mail: kjh75@hanyang.ac.kr
Prof. H.-Y. Lee
Department of Nuclear Medicine
Seoul National University Bundang Hospital
Seongnam, 463-707, Republic of Korea
E-mail: debobkr@gmail.com

DOI: 10.1002/adfm.201203726

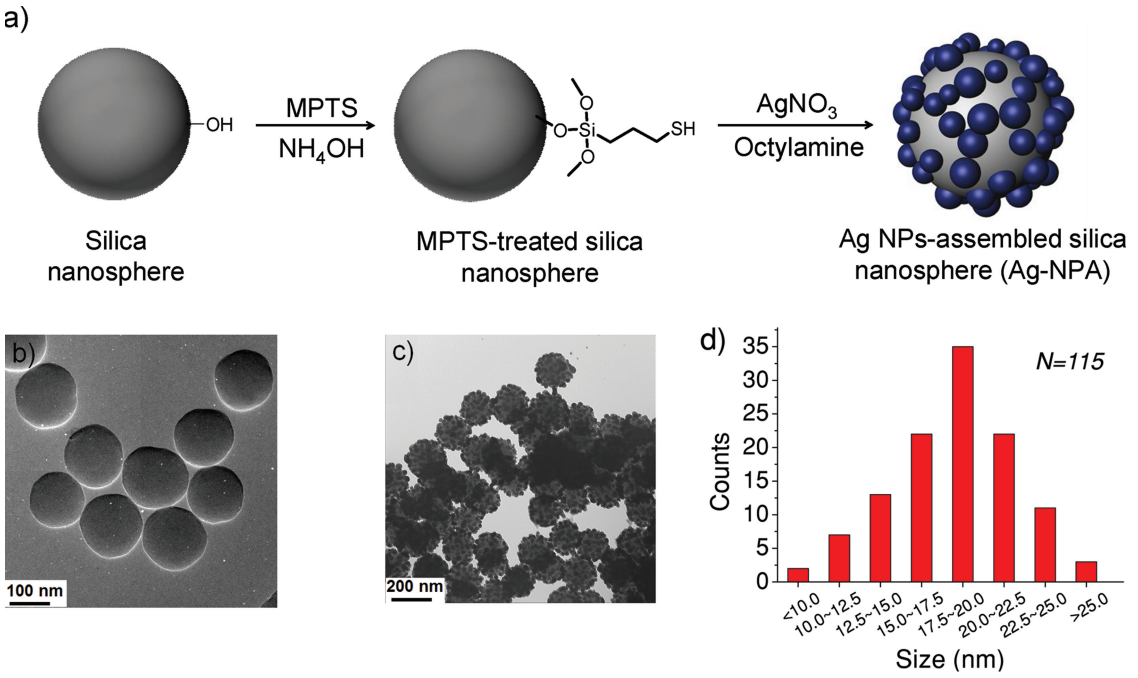

Figure 1. Preparation of Ag nanoparticles-assembled silica nanospheres (Ag-NPAs). a) Schematic diagram for Ag-NPAs using the modified ployol method. TEM images of b) MPTS-treated silica and c) Ag-NPA. d) Size distributions of Ag NPs on the surface of MPTS-treated silica.

Surface-enhanced Raman scattering (SERS) spectroscopy has received growing interest in the field of optical imaging and detection of biological molecules in vivo[7–9,10–13] as well as in vitro.[14] SERS spectroscopy shows great potential as a multiplex detection tool in vivo due to efficient excitation and detection of various distinct Raman labels in the NIR window and the narrow bandwidth of <1 nm.[15–17] SERS spectroscopy also has several advantages such as high signal-to-noise ratio, non-photobleaching features and its use of single photoexcitation.[18,19] Several SERS nanoprobes have been developed for in vivo SERS imaging and therapeutic applications as alternatives to organic fluorescent dyes or QDs. Nie's group[7] and Gambhir's group[8,10] have reported non-invasive SERS imaging and multiplex detection using 60 nm colloidal Au nanoparticles (NPs). To enhance the sensitivity of SERS nanoprobes in in vivo application, several approaches have been presented so far. For instance, optically tuned SERS substrates involving nanorods,[11] hollow nanostructures,[16,17,20] and nanoflowers[21] have been developed to create NIR-active hot spots. Very recently, Raman label compounds, which are more active in the NIR window, have been developed using a combinatorial synthesis technique for in vivo detection of biological molecules.[12] However, strategies for creating nanostructures with SERS hot-spots for signal amplification in NIR window, which are simple, reproducible and scalable, are still required for effective multiplex bio-imaging and in vivo detection of targets. Therefore, designing SERS nanoprobes that are ultrasensitive in the NIR window region is a worthy goal to pursue for effective in vivo and multiplex detection of biological molecules.

Here, we report an approach to develop NIR-sensitive SERS nanoprobes (NIR SERS dots) consisting of the plasmonic Au/Ag hollow-shells (HS) assembled silica nanospheres (Au/Ag HSA) and simple aromatic compounds for in vivo multiplex detection. We modulated the plasmonic band of the Au/Ag HS assemblies using a galvanic replacement reaction, which resulted in a red-shift of their extinction bands from the visible (480 nm) to the NIR region (825 nm). The red-shifted plasmonic extinction of NIR SERS dots enables them to produce more enhanced SERS signals at NIR excitation window (785 nm) than at the visible excitation window (532 nm). The NIR SERS dots produced reproducible and strong NIR-active SERS signals sufficient for single particle detection, which cannot be obtained with single spherical Au NPs. NIR SERS signals from these probes were detectable from 8 mm depth of animal tissues due to these features. Finally, the NIR SERS dots were successfully applied for in vivo multiplex detection by injecting them into live animal tissues, which demonstrated their potential for multiplex detection of specific targets in vivo.

2. Results and Discussion

2.1. Synthesis of Plasmonic Au/Ag Hollow-Shell Assemblies

Au/Ag HS nanostructures exhibit tunable extinction bands from visible to NIR regions (ca. 400–1200 nm),[22,23] indicating that they can be good candidates as SERS-sensitive substrates in the NIR optical window.[19,24] The galvanic replacement reaction, which is well-established method for preparing metallic HS, has ability to finely tune the extinction bands of the Au/Ag HS.[23,25] Plasmonic Au/Ag HSs were fabricated on the surface of silica nanospheres via galvanic replacement reaction of Ag NPs that were pre-assembled on silica to prepare the NIR SERS dots (**Figure 1**). After synthesizing the silica nanospheres

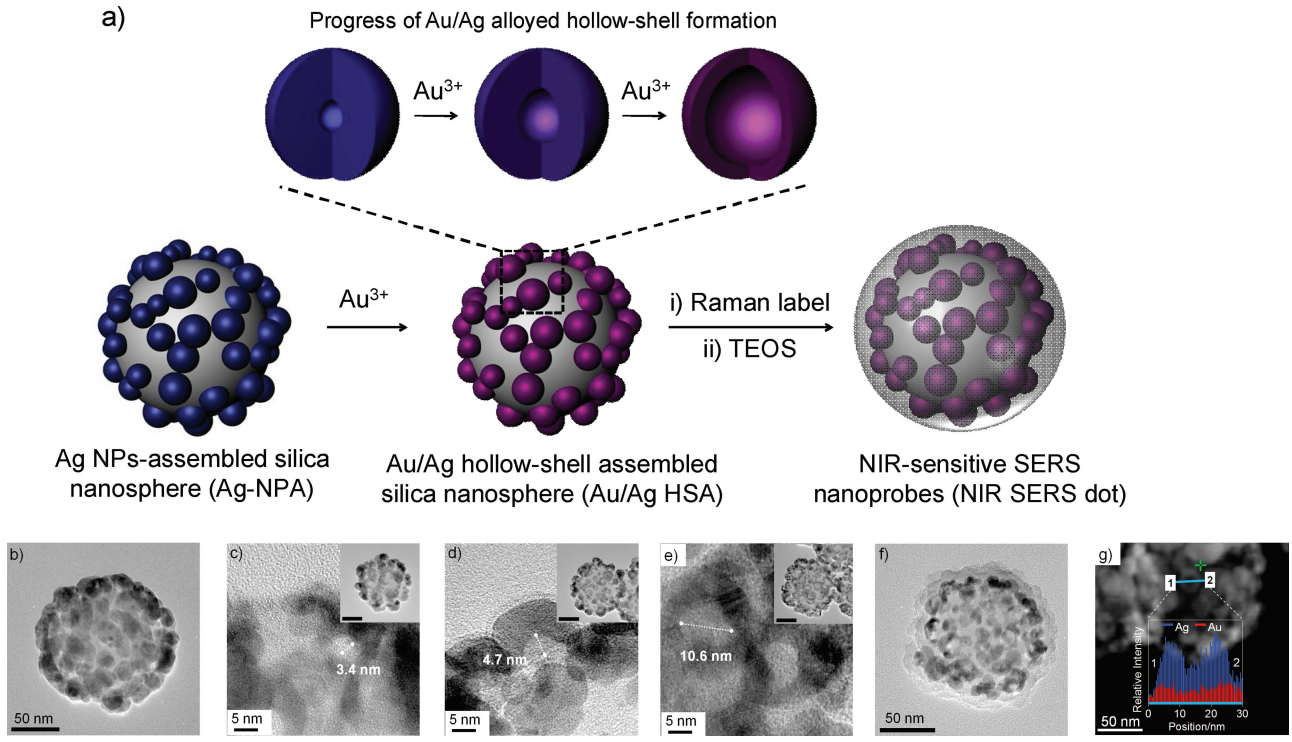

Figure 2. Preparation of Au/Ag HS assembly-based NIR SERS dots. a) Schematic diagram of fabricating the Au/Ag HS assembly-based NIR SERS dots by the galvanic replacement reaction followed by silica encapsulation. TEM images of b) Ag NPs-assembled silica nanosphere (Ag-NPA), and Au/Ag HSs on the silica surface after adding c) 1.0 mL, d) 1.5 mL, and e) 3.0 mL of 0.1 mM-$HAuCl_4$. The hollow interior is represented by a white dotted line in (c–e). The insets are lower magnification TEM images of the Au/Ag HSs assembled silica nanosphere (Au/Ag HSA) (scale bar, 50 nm). f) TEM image of NIR SERS dots (silica shell-coated Au/Ag HSA). g) High angle annular dark field-scanning transmission electron microscopy (HAADF-STEM) image of Au/Ag HSA for Ag and Au atomic profiling of single Au/Ag HS for the sample in (d). The cyan line indicates the atomic profiling region of Au/Ag HSA.

(ca. 125 nm in diameter) using the Stöber method,[26] they were functionalized with thiol groups to directly grow Ag NPs on their surface using the modified polyol method,[27] as shown in Figure 1a. The aliphatic amine (octylamine) was used as both a reducing agent and a stabilizer during this process to grow Ag NPs on the silica surfaces under mild conditions. As shown in Figure 1c, Ag NPs were densely introduced onto the surface of thiol-functionalized silica nanospheres. The number of Ag NPs formed on a single silica nanosphere was 66 ± 12 (counted from 10 silica nanospheres based on their transmission electron microscopy (TEM) images), and their average size was 18.3 nm ± 3.7 nm (counted from 115 Ag NPs, based on their TEM images; Figure 1d).

A $HAuCl_4$ aqueous solution (0.1 mM) was then added using a syringe pump into a 5 mL solution of Ag NPs-assembled silica nanospheres (Ag-NPAs, 0.2 mg/mL) containing poly-*N*-vinyl-2-pyrrolidone (PVP, MW 40 000, 400 mg). The amount of $HAuCl_4$ solution added to the Ag-NPAs was varied from 0.5 to 3.0 mL. **Figure 2**b–e shows the high-resolution TEM (HR-TEM) images of plasmonic Au/Ag HSAs. A small pinhole (< ca. 3 nm) was created on the Ag NPs as 1 mL of $HAuCl_4$ solution was added, while the oxidation of Ag NPs proceeded by Au^{3+} ions at their weakest point (Figure 2c). Then, after adding 1.5 mL of $HAuCl_4$ solution, the size of pinholes increased to about 5 nm, and the Au/Ag hollow nanostructure matured (Figure 2d). In addition, the Au atomic fraction, which was estimated by energy dispersive X-ray spectroscopy (EDX), increased with the added amount of $HAuCl_4$ solution (**Figure 3**a), indicating that an Au/Ag alloy structure had been created on the silica nanospheres. Finally, hollow interiors of 11-nm size in average were formed in the Au/Ag HS on the silica nanospheres as 3.0 mL of $HAuCl_4$ solution was added (Figure 2e). The Au/Ag hollow structures began to change to Au nanosphere structures when more than 3.0 mL of $HAuCl_4$ solution were added, which eventually came off the silica surface (Figure S2, Supporting Information). The structure of the Au/Ag HS on the silica nanospheres was confirmed by atomic profile analysis using scanning transmission electron microscopy (STEM) equipped with an EDX (Figure 2g). According to the atomic line profile analysis results, the intensity of both Au and Ag atoms was higher in the exterior of the nanosphere than that in the interior, further indicating that it had a hollow-shell structure of Au and Ag alloy. The Au/Ag atomic molar composition in Au/Ag HSA has gradually changed to $Au_{0.3}/Ag_{0.7}$ (Figure 3a). This Au/Ag molar composition was consistent with previously reported results for the galvanic replacement reaction.[28]

2.2. Optical Properties of Plasmonic Au/Ag Hollow-Shell Assemblies

Next, we investigated the extinction bands of the plasmonic Au/Ag HSA and their SERS effects. The plasmonic extinction of Au/Ag HSA was red-shifted toward the NIR region

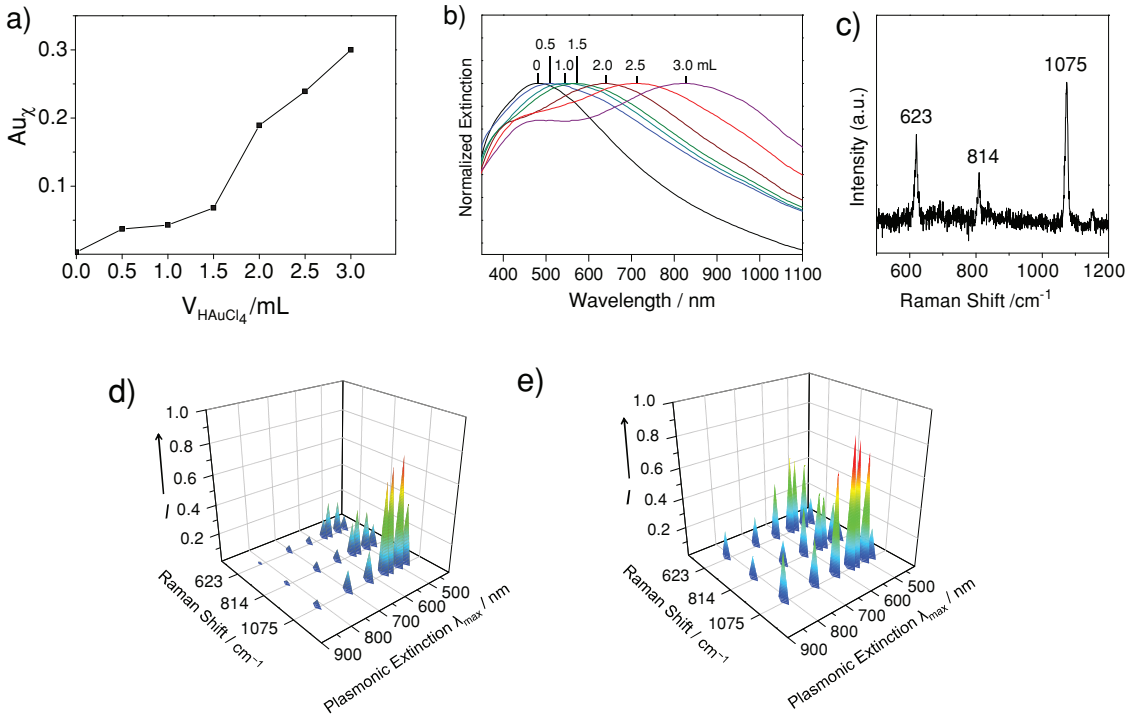

Figure 3. Analysis of Au atomic fraction (Au$_\chi$), plasmonic extinction, and the SERS effect for Au/Ag HSA as a function of different volumes of $HAuCl_4$ solution (0.1 mM): 0, 0.5, 1.0, 1.5, 2.0, 2.5, and 3.0 mL. a) Au atomic fraction and b) the plasmonic extinction spectra of various Au/Ag HSAs with various volumes of $HAuCl_4$ solution. c) Typical SERS spectrum of 4-FBT adsorbed on Au/Ag HSAs. Normalized SERS intensities of 4-FBT adsorbed on various Au/Ag HSAs at 623, 814 and 1075 cm^{-1} by photoexcitation of d) visible light (532 nm wavelength and 2.3 mW laser power) and e) near-infrared (NIR) light (785 nm wavelength and 13 mW laser power). The laser beam diameters at the sample were 2 μm and 3 μm using a 10× objective lens for 532 nm and 785 nm excitations, respectively, and signal acquisition time was 30 s for all measurements.

accompanied by broadening of the extinction band as the added amount of $HAuCl_4$ was increased (Figure 3b). This plasmonic red-shift indicates that the surface plasmon of Au/Ag HSA can be tuned to the NIR window by simply adding the appropriate amount of $HAuCl_4$. The broadening of the plasmonic extinction band can be interpreted by size-heterogeneity of Au/Ag hollow-shells and random plasmonic coupling between hollow-shells of various sizes. In order to find the most active SERS nanoparticles in the NIR window, 4-fluorobenzenethiol (4-FBT) as a labeling compound was adsorbed on the surface of the Au/Ag HSA (this probe is denoted as Au/Ag $HSA_{[4FBT]}$). Each Au/Ag HSA has the unique optical property characterized by extinction maximum λ_{max} ranging from 480 to 825 nm depending on the amount of $HAuCl_4$ solution (Figure 3b). Then, the SERS spectra of Au/Ag $HSA_{[4FBT]}$ were obtained by photoexcitation of two different laser excitation wavelengths: one was 532 nm, which is in the visible range, and the other was 785 nm, which is in the NIR range. Figure 3d,e shows the SERS intensities of Au/Ag $HSA_{[4FBT]}$ at 623, 814, and 1075 cm^{-1} obtained by visible photoexcitation (532 nm) and NIR photoexcitation (785 nm), respectively. The SERS intensities of Au/Ag $HSA_{[4FBT]}$ were normalized with the Raman intensity of the 882 cm^{-1} band of ethanol in order to compensate roughly for the dependency of excitation wavelength.[29] In particular, the Au/Ag HSA with a plasmon extinction of λ_{max} = 565 nm exhibited the strongest SERS intensity by NIR laser excitation, which was more than four times stronger than that of Ag-NPA (Figure 3e and Figure S3 in the Supporting Information). A mismatch of the SERS excitation maximum and the plasmonic extinction maximum is commonly observed,[30] particularly in heterogeneous samples, and this phenomena has been interpreted in terms of heterogeneous nature of SERS hot spots (Supporting Information).[29,31] Taken together, these results show that Au/Ag HSA is a good candidate for a NIR-sensitive SERS nanoprobe, producing a very strong signal in the NIR window.

2.3. Evaluation of Single-Particle SERS Activity

We performed the SERS measurement on a single Au/Ag HSA to further evaluate SERS activity of Au/Ag HSA in the NIR window. After introducing 4-FBT onto Au/Ag HSA, the resulting particles were coated with a silica shell using the modified Stöber method (Figure 2f and Figure S1 in the Supporting Information). The silica shell-coated Au/Ag $HSA_{[4FBT]}$ (NIR SERS $dot_{[4FBT]}$, 0.1 mg/mL in ethanol) solution was drop-cast on a patterned slide glass to measure the SERS signal from single Au/Ag HSA, allowing us to easily distinguish the SERS-measured particles using scanning electron microscopy (SEM) images. After mapping the SERS signals with a 0.5-μm step size for 2 s using a 785-nm laser line, the resulting images were then overlaid with the corresponding SEM images. As shown in **Figure 4**a, the area of intense signals in the SERS intensity map corresponded to the position of the single NIR SERS

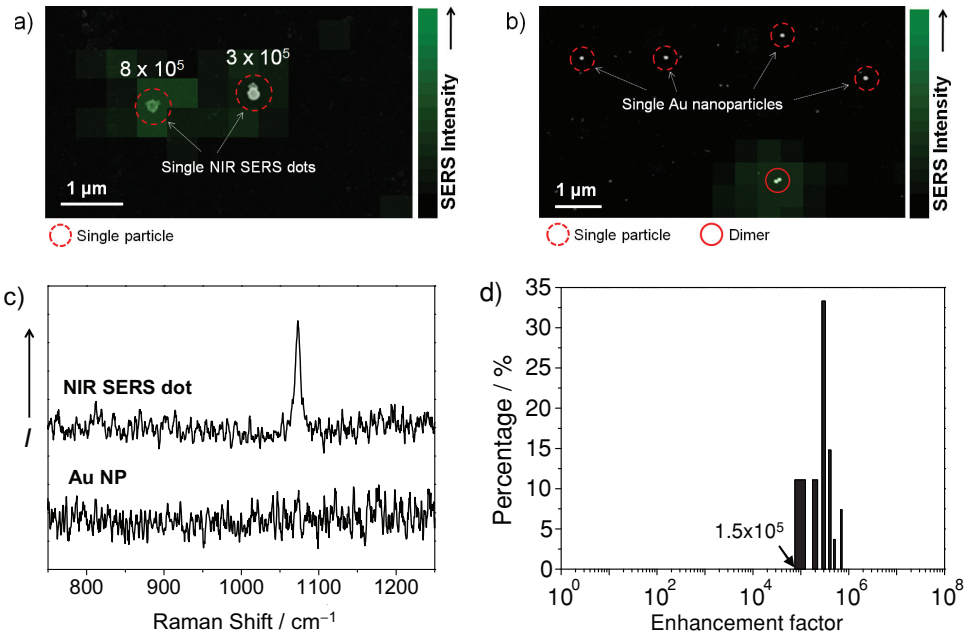

Figure 4. SERS measurements and signal distribution from single NIR SERS dot. a) SERS intensity map of NIR SERS dot bearing 4-FBT (NIR SERS $dot_{[4FBT]}$), showing SERS signals (with enhancement factors of 8×10^5 and 3×10^5): the SERS intensity map was overlaid with its corresponding SEM image. b) SERS intensity map of single Au NPs bearing 4-FBT (Au $NPs_{[4FBT]}$, 80 nm), showing no SERS signals. The solid circle indicates two Au NPs formed a dimer. c) SERS spectra obtained from a single NIR SERS $dot_{[4FBT]}$ and a single Au $NP_{[4FBT]}$. d) Distribution of enhancement factors for the 1075 cm^{-1} Raman band of the NIR SERS $dot_{[4FBT]}$. All measurements were performed with 785 nm photoexcitation of 2.3 mW at sample and acquisition time of 2 s.

$dot_{[4FBT]}$ taken by SEM, indicating that SERS signal is strong enough for each probe particle to be detected (dotted circle in Figure 4a). We also measured the SERS signal from a single Au NP (80 nm, $\lambda_{max} = 548$ nm)[32] to compare their signal intensities. As shown in Figure 4b, the SERS signal from a 4-FBT-coded single Au NP (Au $NP_{[4FBT]}$) was not detectable by NIR excitation (dotted circle in Figure 4b). The SERS signal was detected only when two Au NPs formed a dimer (solid circle in Figure 4b) generating plasmonic coupling between the Au $NPs_{[4FBT]}$. Figure 4c shows the SERS spectra obtained from a single NIR SERS $dot_{[4FBT]}$ and Au $NP_{[4FBT]}$, respectively. These results clearly indicate that the Au/Ag HSA-based SERS nanoprobes exhibit single particle-detectable strong Raman signals in the NIR window. In order to support these experimental results, we calculated the electric field (E-field) enhancements of the Au/Ag HSA and Au NP using the finite element method (FEM) at λ = 785 nm (**Figure 5**a,b) and compared them each other. The dimension of Au/Ag HSA was defined based on the TEM analysis shown in Figure 5a. The calculation revealed that the E-field enhancement was highly localized at the Au/Ag HSA surface, and the field enhancement was maximized at the edge between Au/Ag HSs. The local field enhancement in the Au/Ag HSA was about 10^2 times higher than that in the Au NP (80 nm). Considering that the light intensity is proportional to the square of optical field and incident and scattered fields are enhanced close to the hot spots, these FEM simulations demonstrate why Au/Ag HSA is able to generate strong SERS signals even from a single particle. In addition, we calculated the SERS enhancement factor (EF) for 26 single NIR SERS $dots_{[4FBT]}$ (average SERS EF value, 2.8×10^5) and plotted their distribution (Figure 4d). The distribution of the SERS EF values was very narrow with high reproducibility, which was attributed to the ensemble-average effect of the numerous Au/Ag HSs. This result strongly suggests that the NIR SERS dots can be applied for more accurate and quantitative detection of target biomolecules than previously reported single-hollow particles or NP aggregates.[13,16]

2.4. SERS Signal Penetration Capability of NIR SERS Dots through Animal Tissue

Next, we investigated signal penetration capability of the NIR SERS dots through animal tissues. After the Au/Ag HSA was coated with a silica shell to provide biocompatibility and for easy subsequent functionalization, a 10 μL aliquot of 4-chlorobenzenethiol (4-CBT) coded NIR SERS dots (0.72 nM) was injected into porcine tissues over different injection depths of 1–9 mm. Then, the SERS signals were measured from each depth using a micro Raman system with NIR excitation laser (**Figure 6**a). As expected and shown in Figure 6b, the intensity of the SERS signals decreased with injection depth. Notably a strong SERS signal was still detectable even from an injection depth of 8 mm. These results indicate that the SERS signals generated from NIR SERS dots can be detected sufficiently from deep tissues to be applied to in vivo multiplex detection of target molecules.

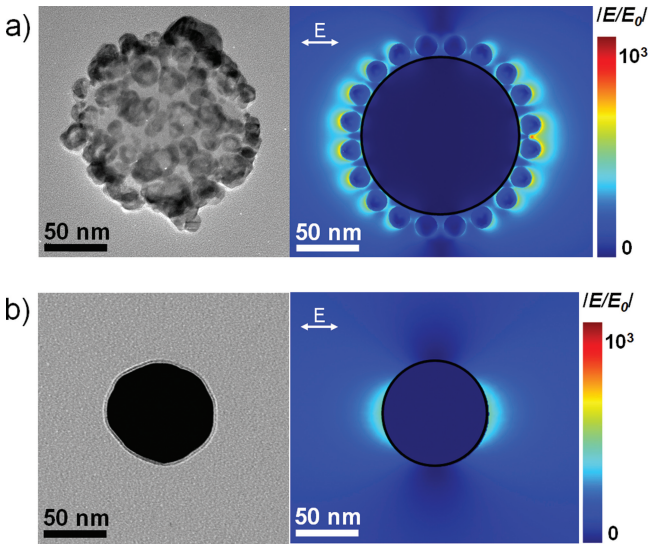

Figure 5. Calculated near-field electromagnetic field distribution of a single Au/Ag HSA and Au NP. a) TEM images and near-field electromagnetic field distribution calculated by FEM for single Au/Ag HSA and b) for single Au NP.

2.5. In Vivo Multiplex Detection of SERS Signal with NIR SERS Dots

Finally, we applied NIR SERS dots to an in vivo multiplex detection in a mouse. NIR SERS dots labeled with simple aromatic compounds, such as 4-aminothiophenol (4-ATP), 4-bromobenzenethiol (4-BBT), 4-CBT and 4-FBT, were prepared for multiplex detection. Each NIR SERS dot had its own characteristic Raman signal, which was much easier to distinguish from mixed signals in a multiplex detection system, particularly when compared to SERS probes using conventional NIR-fluorescent dyes, such as 3,3′-diethylthiatricarbocyanine iodide (DTTC, λ_{max} = 765 nm), which produced complicated Raman fingerprints (Figure S5 in the Supporting Information). Hence, many simple aromatic compounds can be used as Raman label compounds to fabricate NIR SERS dots. This is very advantageous in terms of added multiplexing-capability, cost, and signal deconvolution. A 10 µL aliquot of each NIR SERS dot or their mixture (0.72 nM) was then subcutaneously injected into a nude mouse, as shown in Figure 6c (upper photograph), and their SERS spectra were measured using a micro-Raman system with 785 nm photoexcitation (lower photograph, Figure 6c). As shown

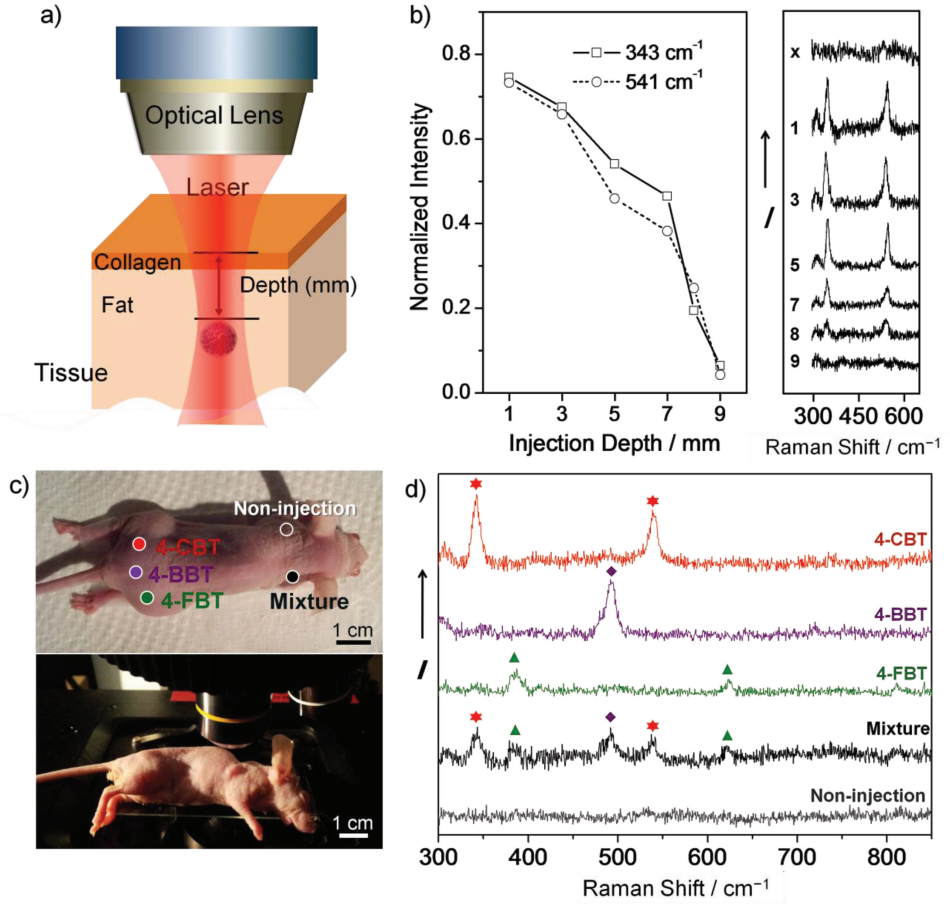

Figure 6. In vivo multiplex detection using NIR SERS dots. a) Schematic illustration of penetration-depth profiling with a 785 nm laser line. b) Normalized SERS intensity and SERS spectra of NIR SERS dots coded with 4-CBT as a function of injection depth (10 s-acquisition and 60 mW laser power). c) Photographs of a mouse in which the NIR SERS dots (4-FBT, 4-CBT, 4-BBT, and their mixture, respectively) were injected (upper) and of the micro-Raman measurement for in vivo multiplex detection (lower). d) SERS spectra from NIR SERS dots injected inside the mouse with the 785 nm photoexcitation of 53 mW laser power and light acquisition time of 100 s.

in Figure 6d, we obatained intense and simple Raman signals for 4-CBT (541 cm^{-1}), 4-BBT (492 cm^{-1}), and 4-FBT (386 cm^{-1}) through the mouse tissues from a mixture of NIR SERS dots as well as from an individual NIR SERS dot. It was also very easy to decode the mixed signals from three different NIR SERS dots. The NIR SERS dots are different from the NIR SERS nanoprobe system using NIR dyes, as they afford intrinsically simple Raman spectra; thus, it is more convenient to deconvolute the mixed signals and to eventually detect several targets from the same area.

3. Conclusions

We have developed NIR SERS nanoprobes based on plasmonic Au/Ag HSA, which produce intense SERS signals in the NIR optical window. A single NIR SERS dot generated strong SERS signals (average EF value 2.8×10^5) with high reproducibility. In addition, the NIR SERS dot signals were detected effectively from deep tissues of up to 8 mm depth, and they exhibited a capability for use in an in vivo multiplex detection system from a live animal study. The high sensitivity, reproducibility and multiplexing-capacity of NIR SERS dots enable them to detect various biological molecules at the same time from a live animal and decipher their unknown functions in a high throughput manner.

4. Experimental Section

Chemicals and Materials: Tetraethylorthosilicate (TEOS), 3-mercaptopropyl trimethoxysilane (MPTS), ethylene glycol, poly(vinyl pyrrolidone) (PVP, MW 40 000), silver nitrate ($AgNO_3$, 99.99+%), octylamine, tetrachloroaurate trihydrate ($HAuCl_4 \cdot 3H_2O$, 99.9+%), 4-aminothiophenol (4-ATP), 4-fluorobenzenethiol (4-FBT), 4-bromobenzenethiol (4-BBT), and 3,3′-diethylthiatricarbocyanine iodide (DTTC) were purchased from Sigma-Aldrich (St. Louis, MO, USA) and used without further purification. Absolute ethanol (99.8%) was purchased from Carlo Erba (Milano, Italy). 4-Chlorobenzenthiol (4-CBT) was purchased from TCI (Tokyo, Japan). Ammonium hydroxide (NH_4OH, 27%), sodium chloride, and ethanol (98%) were purchased from Daejung (Busan, Korea). Gold colloid (80 nm) was purchased from BBInternational (Cardiff, U K). Deionized (DI) water was used for all experiments.

Preparation of Ag Nanoparticles-Assembled Silica Nanosphere (Ag-NPA): TEOS (1.6 mL) was dissolved in 43 mL of absolute ethanol containing ammonium hydroxide (7.5 v/v%), and vigorously stirred for 20 h at 25 °C. The resulting silica nanospheres were centrifuged at 8000 rpm for 15 min and washed with ethanol several times to remove excess reagents. These silica nanospheres were then functionalized with a thiol group. The silica nanospheres (300 mg) were dispersed in 6 mL ethanol containing 300 μL of MPTS and 60 μL of ammonium hydroxide. After the mixture was stirred for 12 h at 25 °C, the MPTS-treated silica nanospheres were centrifuged and washed with ethanol several times. A 100 mg aliquot of MPTS-treated silica nanospheres were thoroughly dispersed in 100 mL of $AgNO_3$ solution (3.5 mM in ethylene glycol). An 82.7 μL aliquot of octylamine was then rapidly added into the dispersed MPTS-treated silica nanospheres. The resulting dispersion was stirred for 1 h at 25 °C. Then, the resulting Ag-NPAs were centrifuged and washed with ethanol several times.

Fabrication of Au/Ag Hollow-Shell Assembled Silica Nanospheres (Au/Ag HSA): A 100 μL aliquot of Ag-NPA (10 mg/mL) was dispersed in 5 mL of PVP (8 wt%, MW 40 000) aqueous solution. A 0.1 mM of $HAuCl_4$ solution was loaded into a disposable plastic syringe (20 mL) with PVC tubing, and was placed on a syringe pump. Portions volumes of 0.1 mM $HAuCl_4$ aqueous solution (0.5, 1.0, 1.5, 2.0, 2.5, and 3.0 mL) were added to the Ag-NPA dispersion at a rate of 0.75 mL/min using the syringe pump. After adding the $HAuCl_4$ solution, the reaction was allowed to stabilize the Au/Ag HS assemblies for 10 min and then cooled to room temperature with vigorous magnetic stirring. The resulting mixture was washed with a saturated solution of NaCl to remove residual AgCl. Then, the resulting suspension was centrifuged and washed with DI water (×3) and ethanol (×3).

Silica Coating of Au/Ag HSA: A 1 mL of Raman label compound (RLC) (2 mM in ethanol) was added to 1 mg of Au/Ag HSA. The resulting dispersion was shaken for 1 h at 25 °C. The Au/Ag $HSA_{[RLC]}$, bearing a self-assembled monolayer of RLC, were transferred to 50 mL of 2-propanol with 1 mg of PVP (MW 40 000). A 2 mL of ammonium hydroxide was added to the reaction mixture under vigorous stirring, followed by the addition of 250 μL of TEOS solution (TEOS/2-propanol, 0.8 v/v%) in four separate portions with a time interval of 30 min. After adding the TEOS, the mixture was allowed to react for 12 h. Then, the resulting mixture was centrifuged at 7000 rpm for 15 min and re-dispersed in ethanol (×5).

Micro-Raman Instrument: Raman measurements were performed using a confocal microscope Raman system (LabRam 300, JY-Horiba, Edison, NJ, USA) equipped with an optical microscope (Olympus, Tokyo, Japan).The Raman scattering signals were collected in a back-scattering geometry and detected by a spectrometer equipped with a thermo-electrically cooled (–70 °C) CCD detector. The excitation laser was focused and the Raman signals were collected by the same open-field 5× or 100× microscope lens (NA 0.90, Olympus). The excitation source was a 785 nm diode laser with 53 or 2.5 mW output power at a sample point for 5× and 100× objective lenses, respectively.

Single-Particle SERS Measurement: SERS intensity of a single NIR SERS $dot_{[4FBT]}$ (Au/Ag $HSA_{[4FBT]}$ with a silica shell) was measured to evaluate SERS activity in the NIR window. The SERS signal of a single Au NP labeled with 4-FBT was also measured for comparison. Au NPs were treated with 4-FBT (2 mM in ethanol) for 1 h at 25 °C. Then, 1 mg of PVP (MW 40 000) was added to the gold NP dispersion. The resulting mixture was shaken for 12 h. The Au NPs were washed three times with ethanol. A patterned slide glass was sonicated in acetone for 20 min and dried by N_2-blowing to eliminate dust on a slide glass and dried. Then, the diluted NP dispersion (0.1 mg/mL in ethanol) was dropped on the patterned slide glass. SERS of the prepared sample was measured by point-by-point mapping with a 0.5 μm step size. All mapping experiments were carried out using a 100× objective lens (NA 0.90) with a 2 s acquisition time. Raman spectra were obtained in a range between 750 and 1250 cm^{-1} using a 785 nm laser. After the Raman measurement, the same area of Raman mapping was observed using field emission-scanning electron microscopy (JSM-6701F, JEOL, Tokyo, Japan) to ensure that only single particles were used for quantification.

Calculation of the SERS Enhancement Factor: SERS enhancement factors (EF) for the NIR SERS $dots_{[4FBT]}$ were estimated using the following equation: $EF = (I_{SERS} \times N_{normal})/(I_{normal} \times N_{SERS})$, where I_{SERS} and I_{normal} are the intensity of the bands from SERS and normal Raman scattering, respectively, and N_{normal} and N_{SERS} are the number of 4-FBT molecules in pure form and self-assembled on the Au/Ag HSA. The peak at 1075 cm^{-1} (for 4-FBT) was used to estimate the EF. Raman signal intensity was measured for both single particles and neat 4-FBT using identical laser power for the EF calculation. Probing volume (18.8 μm^3) was approximated as a cylinder form with a diameter of 2 μm and a height of 6 μm for the normal Raman measurements. N_{SERS} was calculated by geometrically estimating the particle's surface area and a molecular footprint of 4-FBT (0.383 nm^2/molecule),[33] assuming that the thiolate molecules formed a complete monolayer. 4-FBT molecules did not produce any absorption bands that overlapped with the excitation laser wavelength to eliminate the resonance Raman effect.

Theoretical Calculation of Electric Field Enhancement: Finite element method (FEM, COMSOL ver 3.4a Multiphysics software) was used to model Au/Ag HSA suspended in water and to achieve a solution to the Helmholtz wave equation: $\nabla \times (\mu_r^{-1} \nabla \times E) - k_0^2(\varepsilon_r - j\sigma\omega\varepsilon_0)E = 0$. The

calculating mesh structure of Au/Ag HSA was constructed using hybrid mesh generation. The relative permeability of gold and silver were assumed to be $\varepsilon_r = 1$ and the complex permittivity of gold ε_r and silver ε_r were assumed to be a function of wavelength.[34] The model dimension of Au/Ag HSA (silica backbone diameter = 120 nm, Au/Ag HS diameter = 18 nm, Au/Ag HS thickness = 6 nm, and averaged distance between Au/Ag HS surface to Au/Ag HS surface = 8 nm) was based on the TEM analysis as shown in Figure 2. It was assumed that Au/Ag HS was composed of uniformed Au/Ag alloy. The Au/Ag HSA was estimated by a composition-weighted linear combination of the dielectric functions of the metals.[35] The Au/Ag atomic molar composition ($Au_\chi/Ag_{1-\chi}$) on Au/Ag HSA was $Au_{0.07}/Ag_{0.93}$ based on the EDX analysis, and relative permittivity was calculated using the following relationship: $\varepsilon_{Au/Ag} = (\varepsilon_{Au} + 13 \cdot \varepsilon_{Ag})/14$. The polarization vector was typically taken in the parallel direction to the structure of Au/Ag HSA, whereas the direction of the k-vector is taken to be perpendicular to the plane of the structure. A perfectly matched layer and an integration layer, modeled by concentric space, were used to reach perfect absorption at the outer boundary and minimize spurious reflections. The target structure was excited at $\lambda = 785$ nm. The adaptive mesh was refined until the maximum electric field converged. The FEM was used primarily because of its ability to produce adaptive mesh and because it is advantageous over the finite difference time domain (FDTD) method for the complex geometry.[36]

Penetration Depth Profiling: The tissue transparency of NIR SERS dots was investigated using animal tissues. A 10 µL aliquot of NIR SERS $dots_{[4CBT]}$ (0.72 nM in DI water) was injected into porcine tissue at different injection depths (1, 3, 5, 7, 8 and 9 mm) using a 26-gauge needle. The SERS spectra from each injection depth were obtained by changing the focal point from the surface to 10 mm into the tissue at intervals of 1 mm focal depth using the confocal microscope Raman system. All depth profiling was carried out with a 785 nm excitation laser, 53 mW laser power, open-field 5× microscope lens and 10 s acquisition time. The SERS intensities at each injection depth were averaged out from the three strongest SERS spectra. The two 4-CBT peaks (342 and 541 cm^{-1}) were used to evaluate the capability of NIR SERS dots signal penetration. The averaged SERS intensities were normalized with the intensity of the NIR SERS dot suspension (0.72 nM).

In Vivo Multiplex Detection with NIR SERS Dots: Male nude mice were anesthetized with an intraperitoneal injection of ketamine and xylazine mixture solution. The NIR SERS $dot_{[4CBT],\ [4FBT],\ and\ [4BBT]}$ dispersions (in PBS, pH 7.0) were injected subcutaneously into three locations on the gluteal region of the mouse, respectively. The suprascapular area of the mouse was chosen to be subcutaneously injected with a mixture of NIR SERS $dots_{[4CBT],\ [4FBT],\ and\ [4BBT]}$. SERS spectra were obtained from each injection depth (ca. 3 mm) using a micro-Raman system with a 785 nm excitation laser. This study was approved by Seoul National University Bundang Hospital Institutional Animal Care and Use Committee (IACUC No. 64-2011-039).

Supporting Information

Supporting Information is available from the Wiley Online Library or from the author.

Acknowledgements

H.K. and S.J. contributed equally to this work. This research was supported by the Pioneer Research Center Program through the National Research Foundation of Korea funded by the Ministry of Education, Science, and Technology (Grant Number 2012-0000460).

Received: December 17, 2012
Revised: January 28, 2013
Published online: March 13, 2013

[1] a) K. Brindle, *Nat. Rev. Cancer* **2008**, *8*, 94; b) J. K. Willmann, N. van Bruggen, L. M. Dinkelborg, S. S. Gambhir, *Nat. Rev. Drug Discovery* **2008**, *7*, 591.
[2] a) S. K. Lyons, *J. Pathol.* **2005**, *205*, 194; b) X. Montet, V. Ntziachristos, J. Grimm, R. Weissleder, *Cancer Res.* **2005**, *65*, 6330.
[3] R. Weissleder, *Nat. Biotechnol.* **2001**, *19*, 316.
[4] a) R. Weissleder, C. H. Tung, U. Mahmood, A. Bogdanov, *Nat. Biotechnol.* **1999**, *17*, 375; b) H. Kobayashi, Y. Koyama, T. Barrett, Y. Hama, C. A. S. Regino, I. S. Shin, B. S. Jang, N. Le, C. H. Paik, P. L. Choyke, Y. Urano, *ACS Nano* **2007**, *1*, 258.
[5] a) P. W. Barone, S. Baik, D. A. Heller, M. S. Strano, *Nat. Mater.* **2005**, *4*, 86; b) J. H. Kim, D. A. Heller, H. Jin, P. W. Barone, C. Song, J. Zhang, L. J. Trudel, G. N. Wogan, S. R. Tannenbaum, M. S. Strano, *Nat. Chem.* **2009**, *1*, 473; c) K. Welsher, Z. Liu, S. P. Sherlock, J. T. Robinson, Z. Chen, D. Daranciang, H. Dai, *Nat. Nanotechnol.* **2009**, *4*, 773.
[6] a) S. Kim, Y. T. Lim, E. G. Soltesz, A. M. De Grand, J. Lee, A. Nakayama, J. A. Parker, T. Mihaljevic, R. G. Laurence, D. M. Dor, L. H. Cohn, M. G. Bawendi, J. V. Frangioni, *Nat. Biotechnol.* **2004**, *22*, 93; b) H. S. Choi, B. I. Ipe, P. Misra, J. H. Lee, M. G. Bawendi, J. V. Frangioni, *Nano Lett.* **2009**, *9*, 2354.
[7] X. Qian, X. H. Peng, D. O. Ansari, Q. Yin-Goen, G. Z. Chen, D. M. Shin, L. Yang, A. N. Young, M. D. Wang, S. M. Nie, *Nat. Biotechnol.* **2008**, *26*, 83.
[8] C. L. Zavaleta, B. R. Smith, I. Walton, W. Doering, G. Davis, B. Shojaei, M. J. Natan, S. S. Gambhir, *Proc. Natl. Acad. Sci. USA* **2009**, *106*, 13511.
[9] a) D. A. Stuart, J. M. Yuen, N. Shah, O. Lyandres, C. R. Yonzon, M. R. Glucksberg, J. T. Walsh, R. P. Van Duyne, *Anal. Chem.* **2006**, *78*, 7211; b) N. Stone, K. Faulds, D. Graham, P. Matousek, *Anal. Chem.* **2010**, *82*, 3969; c) Y. Wang, J. L. Seebald, D. P. Szeto, J. Irudayaraj, *ACS Nano* **2010**, *4*, 4039.
[10] S. Keren, C. Zavaleta, Z. Cheng, A. de la Zerda, O. Gheysens, S. S. Gambhir, *Proc. Natl. Acad. Sci. USA* **2008**, *105*, 5844.
[11] a) G. von Maltzahn, A. Centrone, J. H. Park, R. Ramanathan, M. J. Sailor, T. A. Hatton, S. N. Bhatia, *Adv. Mater.* **2009**, *21*, 3175; b) J. Qian, L. Jiang, F. Cai, D. Wang, S. He, *Biomaterials* **2011**, *32*, 1601.
[12] a) A. Samanta, K. K. Maiti, K. S. Soh, X. Liao, M. Vendrell, U. S. Dinish, S. W. Yun, R. Bhuvaneswari, H. Kim, S. Rautela, J. Chung, M. Olivo, Y. T. Chang, *Angew. Chem. Int. Ed.* **2011**, *50*, 6089; b) K. K. Maiti, U. S. Dinish, A. Samanta, M. Vendrell, K. S. Soh, S. J. Park, M. Olivo, Y. T. Chang, *Nano Today* **2012**, *7*, 85.
[13] M. V. Yigit, L. Zhu, M. A. Ifediba, Y. Zhang, K. Carr, A. Moore, Z. Medarova, *ACS Nano* **2011**, *5*, 1056.
[14] a) W. E. Doering, S. Nie, *Anal. Chem.* **2003**, *75*, 6171; b) D. S. Grubisha, R. J. Lipert, H. Y. Park, J. Driskell, M. D. Porter, *Anal. Chem.* **2003**, *75*, 5936; c) S. P. Mulvaney, M. D. Musick, C. D. Keating, M. J. Natan, *Langmuir* **2003**, *19*, 4784; d) G. L. Liu, Y. Lu, J. Kim, J. C. Doll, L. P. Lee, *Adv. Mater.* **2005**, *17*, 2683; e) J. H. Kim, J. S. Kim, H. Choi, S. M. Lee, B. H. Jun, K. N. Yu, E. Kuk, Y. K. Kim, D. H. Jeong, M. H. Cho, Y. S. Lee, *Anal. Chem.* **2006**, *78*, 6967; f) J. Kneipp, H. Kneipp, M. McLaughlin, D. Brown, K. Kneipp, *Nano Lett.* **2006**, *6*, 2225; g) S. Schlücker, B. Küstner, A. Punge, R. Bonfig, A. Marx, P. Ströbel, *J. Raman Spectrosc.* **2006**, *37*, 719; h) S. Lee, S. Kim, J. Choo, S. Y. Shin, Y. H. Lee, H. Y. Choi, S. Ha, K. Kang, C. H. Oh, *Anal. Chem.* **2007**, *79*, 916; i) M. Y. Sha, H. Xu, M. J. Natan, R. Cromer, *J. Am. Chem. Soc.* **2008**, *130*, 17214; j) B. H. Jun, M. S. Noh, J. Kim, G. Kim, H. Kang, M. S. Kim, Y. T. Seo, J. Baek, J. H. Kim, J. Park, S. Kim, Y. K. Kim, T. Hyeon, M. H. Cho, D. H. Jeong, Y. S. Lee, *Small* **2010**, *6*, 119; k) K. Kim, J. Y. Choi, H. B. Lee, K. S. Shin, *ACS Appl. Mater. Interfaces* **2010**, *2*, 1872; l) J. F. Li, Y. F. Huang, Y. Ding, Z. L. Yang, S. B. Li, X. S. Zhou, F. R. Fan, W. Zhang, Z. Y. Zhou, D. Y. Wu, B. Ren, Z. L. Wang,

Z. Q. Tian, *Nature* **2010**, *464*, 392; m) A. Pallaoro, G. B. Braun, N. O. Reich, M. Moskovits, *Small* **2010**, *6*, 618; n) J. H. Kim, H. Kang, S. Kim, B. H. Jun, T. Kang, J. Chae, S. Jeong, J. Kim, D. H. Jeong, Y. S. Lee, *Chem. Commun.* **2011**, *47*, 2306.

[15] a) L. Sun, C. Yu, J. Irudayaraj, *Anal. Chem.* **2007**, *79*, 3981; b) B. R. Lutz, C. E. Dentinger, L. N. Nguyen, L. Sun, J. Zhang, A. N. Allen, S. Chan, B. S. Knudsen, *ACS Nano* **2008**, *2*, 2306.

[16] B. Küstner, M. Gellner, M. Schütz, F. Schöppler, A. Marx, P. Ströbel, P. Adam, C. Schmuck, S. Schlücker, *Angew. Chem. Int. Ed.* **2009**, *48*, 1950.

[17] M. Sanles-Sobrido, W. Exner, L. Rodríguez-Lorenzo, B. Rodríguez-González, M. A. Correa-Duarte, R. A. Álvarez-Puebla, L. M. Liz-Marzán, *J. Am. Chem. Soc.* **2009**, *131*, 2699.

[18] a) W. E. Doering, M. E. Piotti, M. J. Natan, R. G. Freeman, *Adv. Mater.* **2007**, *19*, 3100; b) B. H. Jun, G. Kim, M. S. Noh, H. Kang, Y. K. Kim, M. H. Cho, D. H. Jeong, Y. S. Lee, *Nanomedicine* **2011**, *6*, 1463.

[19] S. Schlücker, *ChemPhysChem* **2009**, *10*, 1344.

[20] X. W. Liu, J. Lin, T. F. Jiang, Z. F. Zhu, Q. Q. Zhan, J. Qian, S. He, *Prog. Electromagn. Res.* **2012**, *128*, 35.

[21] J. Xie, Q. Zhang, J. Lee, D. Wang, *ACS Nano* **2008**, *2*, 2473.

[22] a) S. Oldenburg, R. Averitt, S. Westcott, N. Halas, *Chem. Phys. Lett.* **1998**, *288*, 243; b) J. Jackson, N. Halas, *J. Phys. Chem. B* **2001**, *105*, 2743; c) M. Gellner, B. Küstner, S. Schlücker, *Vib. Spectrosc.* **2009**, *50*, 43.

[23] S. E. Skrabalak, L. Au, X. Li, Y. Xia, *Nat. Protocols* **2007**, *2*, 2182.

[24] R. A. Alvarez-Puebla, D. J. Ross, G. A. Nazri, R. F. Aroca, *Langmuir* **2005**, *21*, 10504.

[25] J. Chen, B. Wiley, Z. Y. Li, D. Campbell, F. Saeki, H. Cang, L. Au, J. Lee, X. Li, Y. Xia, *Adv. Mater.* **2005**, *17*, 2255.

[26] W. Stöber, A. Fink, E. Bohn, *J. Colloid Interface Sci.* **1968**, *26*, 62.

[27] H. Kang, T. Kang, S. Kim, J. H. Kim, B. H. Jun, J. Chae, J. Park, D. H. Jeong, Y. S. Lee, *J. Nanosci. Nanotechnol.* **2011**, *11*, 579.

[28] D. Seo, H. Song, *J. Am. Chem. Soc.* **2009**, *131*, 18210.

[29] R. A. Álvarez-Puebla, *J. Phys. Chem. Lett.* **2012**, *3*, 857.

[30] a) A. M. Michaels, M. Nirmal, L. Brus, *J. Am. Chem. Soc.* **1999**, *121*, 9932; b) S. L. Kleinman, E. Ringe, N. Valley, K. L. Wustholz, E. Phillips, K. A. Scheidt, G. C. Schatz, R. P. Van Duyne, *J. Am. Chem. Soc.* **2011**, *133*, 4115; c) S. Abalde-Cela, S. Ho, B. Rodríguez-González, M. A. Correa-Duarte, R. A. Álvarez-Puebla, L. M. Liz-Marzán, N. A. Kotov, *Angew. Chem. Int. Ed.* **2009**, *48*, 5326.

[31] Y. Fang, N. H. Seong, D. D. Dlott, *Science* **2008**, *321*, 388.

[32] P. N. Njoki, I. I. S. Lim, D. Mott, H. Y. Park, B. Khan, S. Mishra, R. Sujakumar, J. Luo, C. J. Zhong, *J. Phys. Chem. C* **2007**, *111*, 14664.

[33] P. Jiang, K. Deng, D. Fichou, S. S. Xie, A. Nion, C. Wang, *Langmuir* **2009**, *25*, 5012.

[34] P. G. Etchegoin, E. C. Le Ru, M. Meyer, *J. Chem. Phys.* **2006**, *125*, 164705.

[35] E. Hao, G. C. Schatz, *J. Chem. Phys.* **2004**, *120*, 357.

[36] T. Grosges, A. Vial, D. Barchiesi, *Opt. Express* **2005**, *13*, 8483.